

## GAUSSIAN GROOVES PROPAGATING ACROSS A MOVING CURVED INTERFACE IN DIRECTIONAL SOLIDIFICATION

P. E. Cladis

*Advanced Liquid Crystal Technologies, POB 1314, Summit, NJ 07902 USA*

### *Abstract*

In gratitude to Antoine Skoulios for original and illuminating insights on complex materials, and, to celebrate the emergence of his new adventures, this article is a synopsis of astonishing observations made about a decade ago on a deceptively simple material, succinonitrile, during its crystal growth from a curved phase boundary traveling in narrow channels. For a range of pulling speeds,  $v$ ,  $v_{c1} < v < v_{c2}$ , the flat interface transforms, first, to a curved one, then, to a cellular one by groove propagation. The shape of the lead groove is Gaussian, consistent with a linear concentration gradient across the interface, and the pattern has a well-defined wavelength. When  $v < v_{c1}$ , the interface remains flat and when  $v > v_{c2}$ , the pattern is time dependent.

PACS: 81.30.Fb, 61.50.Cj, 05.70.Ln

### INTRODUCTION

This article describes astonishing observations made about a decade ago [1-3] on a deceptively simple material, succinonitrile,  $C_4H_4N_2$ : waxy isomeric crystals that melt at  $57.15^\circ\text{C}$ , during its crystal growth from an asymmetric interface in a narrow channel.

Succinonitrile is the material used to study the crystal growth processes in directional solidification (Fig. 1) because its solid-liquid interface is not faceted i.e. is “rough”, and therefore is flat in a temperature gradient [4]. Such interfaces are important as many technologically important metals and semiconductors exhibit rough interfaces.

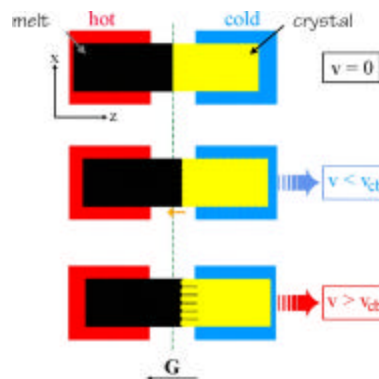


**Fig. 1.** Classical directional solidification where the solid-liquid phase boundary is perpendicular to a temperature gradient,  $G$ . A flat phase boundary (*top*) is forced to travel towards the hot contact by pulling the sample from the hot contact to the cold one (*middle*). Above a critical pulling speed,  $v_{cb}$ , the flat interface develops a pattern (*bottom*).



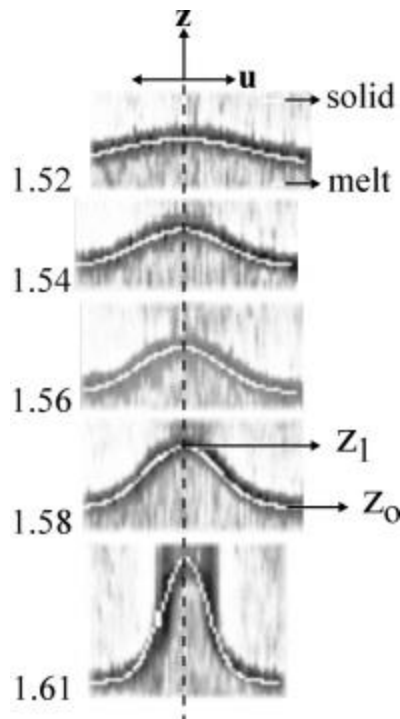


**Fig. 2.** Groove evolution on a traveling asymmetric interface.  $v=1\mu\text{m}/\text{s}$ . Taking the groove center at  $u = 0$ ,  $Z_1(u,t)$  is the interface between the solid and its melt. Pulling distance,  $d(\text{mm}) = d_0 + vt$ , is on the left of the figures. The groove amplitude is zero at  $d_0 = 1.51\text{mm}$ . When the groove becomes 3-dimensional ( $1.59 < d < 1.61\text{mm}$ ), a new groove replaces it as pattern leader. The fits to Gaussians are the overlaid white lines.

in liquid crystal x-ray diffraction, we were fascinated by “grooves” traveling across a curved interface. We thought they looked Gaussian (Fig. 2). We believe Gaussian grooves are triggered by the installation of a curved interface asymmetric about  $\mathbf{G}$  [1-3].

## DIRECTIONAL SOLIDIFICATION

In classical directional solidification [4] (Fig. 1), a transparent alloy is placed in a temperature gradient,  $\mathbf{G}$ , so that temperature is mapped onto a spatial dimension,  $\mathbf{z}$ . The solid-liquid interface, a surface of constant temperature, is at the

In principle, small amplitude periodic perturbations of a rough interface can continuously evolve making them more amenable for developing theoretical insight into universal macroscopic features of crystal growth. As succinonitrile is transparent, the evolution of its interfacial profile may be followed with a video-camera and computerized image processing.

Directional solidification is a way to control traveling phase transition boundaries [4] and so study quantitatively the types of structures that can arise in non-linear, non-equilibrium dissipative systems [5]. About a decade ago, there was a surge in activity towards developing conceptual frameworks for predicting the dynamic behavior of such systems that can range from steady coherent structures to fully developed turbulence.

In the case of the solid-liquid interface, most of the theoretical work has been on the development of small “bumps” on the flat interface. However, influenced by early work with Daniel Guillon on the evolution of line-shapes

melting temperature,  $T_M$ . In profile, the flat interface is a straight line. The crystal is forced to grow by pulling the sample at a constant speed,  $\mathbf{v} \parallel \mathbf{G}$ , towards a cold contact. Above a critical pulling speed [7],  $v_{cb}$ , the flat interface becomes unstable to a “cellular interface”, the pattern. Now, parts of the interface are at higher temperatures than  $T_M$ , called “tips”, and parts at a lower temperature than  $T_M$ , called “grooves”. The wavelength of the patterns are typically,  $\lambda \sim 100\mu\text{m}$ . The outstanding question in pattern formation is: what determines  $\lambda$ ?

There is no known mechanism to account for pattern formation when the material is pure [8]. In the conventional scenario, the balance between impurity rejection by the growing crystal and impurity diffusion away from the interface into the liquid, creates an exponentially decaying impurity gradient in advance of the moving interface. From the linear diffusion equation, the impurity gradient in advance of the interface defines a dynamic length scale,  $l_D \equiv D/v \sim 500\mu\text{m}$  with diffusion constant,  $D \sim 1 \times 10^{-5} \text{cm}^2/\text{s}$  and  $v \sim 2\mu\text{m}/\text{s}$ .

When  $v < v_{cb}$ , the impurity distribution across the interface is uniform and the interface profile is a straight line. With increasing rate of crystal growth (increasing  $v$ ) the impurity gradient becomes steeper as  $l_D$  decreases. When  $l_D$  is smaller than the equilibrium liquidus slope ( $v > v_{cb}$ ) material on the solid side of the interface is in contact with liquid at a lower temperature than the equilibrium liquidus temperature. A small perturbation of the solid into the liquid can then overcome stabilizing influences of the temperature gradient at long wavelengths and surface forces at short wavelength to render the flat interface unstable.

In our experience, patterns formed by succinonitrile’s traveling solid-liquid interface typically had a very broad range of  $\lambda$ ’s, the grooves are very deep (extend to very low temperatures) and the mean interface temperature consistently moved to increasingly lower temperatures (no steady state) throughout an experiment [9].

#### BREAKING INTERFACIAL PARITY

For these experiments, succinonitrile is vacuum loaded into a flat glass capillary: width,  $L = 1\text{--}2\text{mm}$ ; thickness,  $100\mu\text{m}$ ; length,  $50\text{mm}$ , then sealed. Measurements are made using a high-resolution directional solidification apparatus [10] and defect free seed-crystals [11]. In our geometry, then, the crystal is forced to grow in a relatively narrow channel:  $L = 1\text{--}2\text{mm} \sim 10\text{--}20\lambda$ .

The sample is placed in the temperature gradient ( $G = 7.5\text{K}/\text{mm}$ ) so that the capillary long axis is at a small angle (less than  $3^\circ$ ) to  $\mathbf{G}$  (Fig. 3).



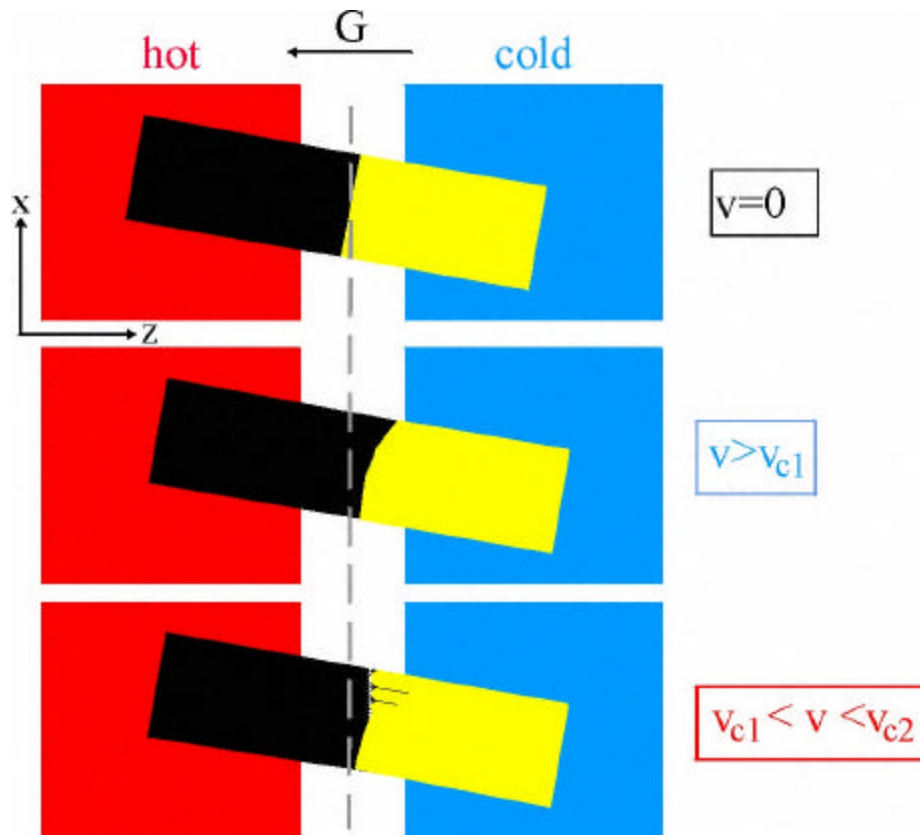


**Fig. 3.** Schematic of an  $[x, z]$  plane of the experimental geometry viewed along  $y$ , the thinnest dimension of the capillary,  $100\mu\text{m}$ . Forcing the interface, not perpendicular to  $v\|\mathbf{G}$ , to grow in a narrow channel ( $L\sim 1\text{-}2\text{mm}$ ) leads to a curved interface (*middle*) and groove propagation (*bottom*). Both  $\mathbf{G}$  and  $\mathbf{v}$  are  $\perp$  to the edges of the hot and cold contacts. The capillary is at a small angle to  $\mathbf{G}$ , exaggerated here but in the experiment  $\sim 1.5\text{-}3^\circ$ . While the dotted line tangent to the cell tips is  $\perp$  to  $\mathbf{G}\|\mathbf{v}$ , groove axes are parallel to the side-walls.

In our apparatus, the maximum pulling distance, effected by a stepping motor (smallest step-size  $0.1\mu\text{m}$ ), is  $d_{\text{max}} = 25\text{mm}$ . A frequency generator controls step-rate to 1 part in  $10^6$ . The separation between hot and cold contacts is  $4\text{mm}$ .

A high speed imaging system records the  $x$ - $z$  plane through an automated video system attached to an optical microscope observing the interface along its smallest dimension, the  $y$ -axis. Grain boundary free seed crystals are obtained by repeatedly freezing then melting the sample in  $\mathbf{G}$ . In addition, interface position measurements during melting give a value for the "dynamical" partition coefficient,  $k$ , of  $0.6$  (assuming a liquid impurity diffusion constant,  $D = 1.0 \times 10^{-5}\text{cm}^2/\text{s}$  [8]). We note that for  $k > 0.45$ , the planar-cellular bifurcation is predicted to be su-

percritical (continuous) [12].

We determine  $v_{cb}$  by measuring the pulling distance,  $d_u$ , for the onset of the cellular pattern at different pulling speeds,  $v$  [11], then, plot  $1/d_u$  vs.  $v$  to obtain a "bulk" critical pulling speed,  $v_{cb} = 1.12\mu\text{m/s}$  at  $1/d_u = 0$ .

OBSERVATIONS AND MEASUREMENTS

When solidification begins with  $v \sim v_{cb}$ , the amplitude,  $A$  (defined in Fig. 4), of a longwavelength perturbation of the flat interface, increases from zero, peaks at  $A_{max}$ , then, decreases when the first groove begins to form (Fig. 4).  $A$  only grows while there are no grooves, i.e.  $d < d_u$ .  $A_{max}$  decreases linearly with  $v$ , is independent of sample width and is zero when  $v = v_{c2} = 2.9\mu\text{m/s}$  (inset Fig. 4).

Our interpretation is the following [1-3]. At rest, to minimize surface energy, the solid-liquid interface profile,  $Z_1(x,0)$ , of succinonitrile is  $\perp$

to the capillary side-walls - not  $\mathbf{G}$  - when the capillary is sufficiently narrow and at a small angle ( $1.5\text{-}3^\circ$ ) to  $\mathbf{G}$  (Fig. 3). This sets up a linear concentration gradient across the interface. When solidification begins with  $\mathbf{v} \parallel \mathbf{G}$  and before the formation of any grooves ( $d < d_u$ ), an impurity flux develops across the interface leading to a further increase in impurity concentration at the colder end of the interface where it becomes unstable first (Figs. 3 and 5).

When  $d_u$  is large [11],  $A_{max}$  is large. When  $v > 3v_{cb}$ , the planar-cellular transition occurs simultaneously everywhere on the interface, the effect is not observed and the pattern is time-dependent.

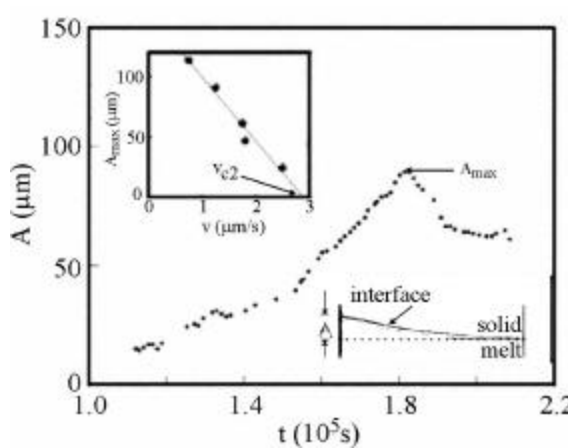


**Fig. 4.** At very small growth speeds, the initially flat interface becomes curved (*bottom inset*).  $A$  is the difference between the minimum and maximum values of the interface temperature. The vertical lines are shadows from the capillary side-walls and the horizontal dotted line is  $\parallel$  the interface rest profile. In the main figure, measurements of  $A$  vs. time,  $t$  for  $v = 1.25\mu\text{m/s}$ . At  $A_{max}$ , the first groove forms. The smaller graph shows  $A_{max}$  vs.  $v$ .



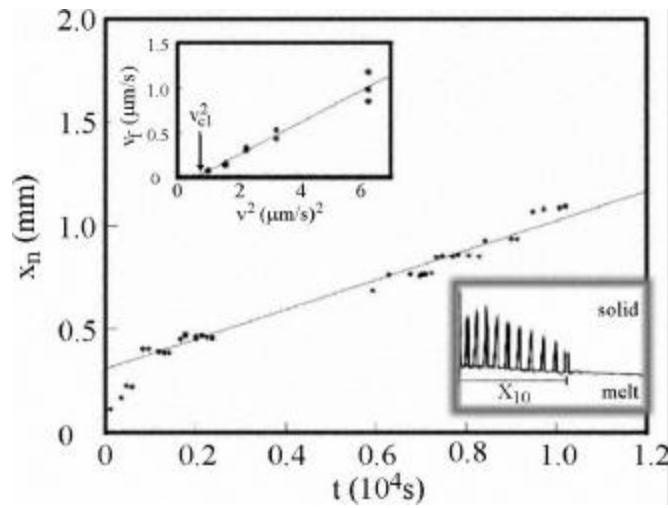


**Fig. 5.** Determination of the front speed,  $v_f$ ; position of the groove that leads the propagating pattern ( $x_n$ ) as a function of time.  $v = 1\mu\text{m/s}$ .  $v_f$  is different near the capillary edges. The gap in the data is where the magnification was increased to study the groove evolution in more detail (e.g. Fig. 5). *Smaller graph:* Front speed,  $v_f$  vs  $v^2$ . The slope is  $\sim 2\lambda/D \pm 20\%$  i.e.  $v_f \approx 2\lambda(v^2 - v_{cl}^2)/D$ . *Inset:* Digitally enhanced image of cell pattern.  $x_{10}$  is the distance from the side walls to the center of the 10<sup>th</sup> groove to form.

When  $v > v_{cl}$ , grooves of liquid propagate [13] from the colder end of the interface to the warmer end (Fig. 5) at speed  $v_f$ . The grooves are parallel to the long axis of the capillary so their centers,  $x_n$ , are fixed. However, the common tangent of the cell tips is  $\perp \mathbf{v}$ , so the cell pattern is asymmetric (Figs. 3 and 5). When  $v = 1\mu\text{m/s}$ , the time between successive groove formation (Fig. 5) is

approximately  $\tau \equiv D/v^2$  whereas at  $v = 2.5\mu\text{m/s}$ , it is closer to  $\tau/2$ . The smaller graph in Fig. 5 shows  $v_f$  as a function of  $v^2$ . The slope of the best line is  $2\lambda/D \pm 20\%$ , i.e.  $v_f \approx (2\lambda/D)(v^2 - v_{cl}^2)$  giving  $v_{cl} = 0.8\mu\text{m/s}$ .

When  $0 < v < v_{cl}$ , grooves do not occur. When  $v_{cl} < v < v_{c2}$ , power spectra of the groove patterns have a sharp peak at a  $\lambda = 2\pi/q_0$  that varies from  $81 \pm 3\mu\text{m}$  at  $v = 1\mu\text{m/s}$  to  $70 \pm 2\mu\text{m}$  at  $v \approx v_{c2}$ . In contrast, the spectra for time dependent patterns when  $v > v_{c2}$  are too broad to determine  $\lambda$  [1-3].

### ANALYSIS OF GROOVE PROFILES

Since grooves form sequentially in the propagating pattern and their position is fixed, we analyzed the shape,  $(Z_1(x,t))$ , of the lead groove in the pattern, i.e. the groove forming next to the planar state (Fig. 2). When  $v_{cl} < v < v_{c2}$  and as a function of time, its shape is well-described by nearly self-similar Gaussians in  $x$ .

Fig. 2 shows the evolution of a lead groove when  $v = 1\mu\text{m/s} \sim v_{cl}$ . We digitized and fitted  $Z_1$  to inflating Gaussians,  $Z_1 = Z_1 - Z_0 = f_1(t)f$  where  $f = \exp(-u^2/2\xi_0^2)$ ,  $u = x - x_n$  and  $x_n$  is the center of the  $n^{\text{th}}$  groove. The fit parameters,  $f_1$  and

$\xi_0$ , depend on time while  $x_n$  and  $z_0$  do not. The fitting error is  $\sim 5\%$ . When  $t \approx \tau \equiv D/v^2$ , a new groove starts, correlating with jumps in both  $\xi_0$  and  $f_1$  (Fig. 6) as well as the onset of 3-d effects (Fig. 5) in the retiring groove. This suggests that a stationary pattern of Gaussian grooves (i.e. no 3-d effects [14]) may be stabilized in thinner samples.

When  $t < \tau$ , the groove amplitude is controlled by impurity diffusion and  $f_1 \xi_0^2$  is nearly constant. Also, when  $\tau > t > \tau/5$ ,  $Z_1/f_1 \approx f$ , with  $f$  nearly independent of time: the Gaussians in Fig. 2 are nearly "self-similar".

Taking all the measured points,  $\langle \xi_0 \rangle = 16.2 \mu\text{m}$ , and  $\lambda$  is approximately given by:

$$\lambda \approx \int_{-\infty}^{\infty} f \, du = 2(2\pi)^{1/2} \langle \xi_0 \rangle.$$

Thus, when the overlap between the Gaussian of a groove and its predecessor (or successor) is small, a pattern with a well-defined  $\lambda$  is established. When overlap is significant, e.g., when  $v > v_{c2}$ ,  $\lambda$  is not well-defined and the pattern is time dependent [1-3].

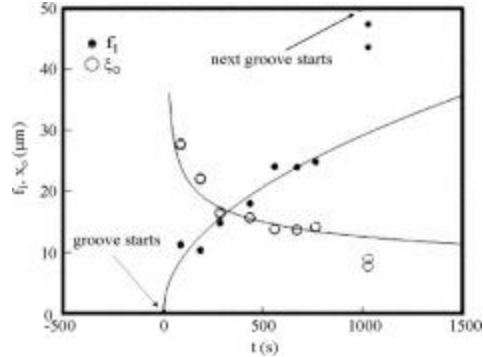


**Fig. 6.** Time dependence of the amplitude,  $f_1$  (o) and width,  $\xi_0$  (•) from the fits in Fig. 5. The jumps in  $\xi_0$  and  $f_1$  correlate with the start of the next groove.

### WAVELENGTH SELECTION AND GAUSSIAN GROOVES

Wavelength selection mechanisms in directional solidification are not well understood. Indeed, when the neutral stability curve is flat ( $k$  is small), there are predictions [15] of no wavelength selection because of mode-coupling between harmonics and sub-harmonics of some selected wavelength,  $\lambda$ . This description [15] qualitatively agrees with observations for  $v > v_{c2}$  [1-3].

However, some mechanisms have been shown to lead to wavelength selection in other pattern forming systems. Three such mechanisms are front propagation [16], "soft boundary conditions" where the control parameter is "ramped" (spatially varied from above to below threshold) [17] and "parity breaking" [18].

Existing front propagation theories do not describe the observed dependence of front speed,  $v_f$ , on pulling speed,  $v$  (Fig. 5). While the stationary pattern of cells with groove depth monotonically decreasing as grooves propagate across the in-



terface (Fig. 5) is reminiscent of a ramp, calculations of wavelength selection in a ramp are for a supercritical bifurcation and a specific geometry [19].

Here, we observe features associated with a subcritical bifurcation such as; the finite value of  $dv_f/dv$  at  $v = v_{c1}$ , presence of deep grooves (no sinusoidal pattern near onset [20]), coexistence of planar and cellular states for  $v < v_{c2}$  (Fig. 5) and the fact that the front propagates both ways [21]. There are also features of a forced parity breaking transition [18] (Fig. 4). Although the pattern is asymmetric, the groove envelope propagates, not groove positions, and it is the first instability, not a secondary one launched from a steady state periodic pattern [22].

Interpreting the initial linear concentration gradient as a ramp with control parameter,  $\varepsilon$  for the instability onset, linear in  $x$ :  $\varepsilon = -\alpha_0(x-x_0)$ , then, to first order in  $Z_1$ ,  $dZ_1/dt \sim \varepsilon Z_1$ . For a perturbation traveling across the interface,  $dZ_1/dt = v_f dZ_1/dx \sim -\alpha_0(x-x_0) Z_1$  which, on integration, gives a Gaussian profile for  $Z_1$ . Thus, Gaussian grooves are consistent with a ramp set-up by an initially asymmetric interface.

## CONCLUSIONS

If initially in a narrow capillary, the interface is not  $\perp(\mathbf{v}||\mathbf{G})$  (Fig. 3), two new critical speeds,  $v_{c1}$  and  $v_{c2}$  emerge (Figs. 4 and 5). When  $v_{c1} < v < v_{c2}$ , front propagation ( $v_f \propto v^2$ ) along a curved interface ( $A \neq 0$ ), leads to an asymmetric cell pattern with wavelength selection. When  $0 \leq v < v_{c1}$ , grooves do not form and when  $v > v_{c2}$ , they appear all at once:  $\lambda$  is not well-defined and the pattern is time dependent. When  $v \sim v_{c1}$  the shape of the lead groove is well-described by Gaussians with amplitude,  $f_1 \sim 1/\xi_0^2$ .  $\xi_0$  is nearly constant when  $\tau/5 < t < \tau$  so the Gaussians are nearly self-similar. Furthermore,  $\xi_0 \approx 16.2\mu\text{m} \approx \lambda/2(2\pi)^{1/2}$ : when overlap between the lead groove and its predecessor/successor is small,  $\lambda$  is well-defined.

We have presented a feast with a mind-boggling bazaar of aromas and flavors to tempt the adventurous, discriminating but nevertheless integrating palate of Antoine Skoulios.

Χρόνια Πολλά!

## REFERENCES

- [1] P. E. Cladis, J. T. Gleeson and P. L. Finn in *Non-linear Evolution of Spatio-Temporal Structures in Dissipative Continuous Systems*, F.



- Busse and L. Kramer (eds), Plenum Press (1990); *Non-linear Structures in Physical Systems - Pattern Formation, Chaos and Waves*, Lui Lam and Hedley C. Morris (eds), Springer Verlag(1990).
- [2] P. E. Cladis, J. Stat. Phys., **64**, 1103 (1991).
- [3] J. T. Gleeson, P. L. Finn and P. E. Cladis, Phys. Rev. **A45**, 8719 (1992).
- [4] K. A. Jackson and J. D. Hunt, Acta. Metall. **13**, 1212 (1965).
- [5] J. S. Langer, Rev. Mod. Phys. **52**, 1 (1980); in *Chance and Matter*, J. Souletie, J. Vannimenus and R. Stora (eds), Elsevier (New York) 1986 p. 629; Science **243**, 1150 (1989).
- [6] *Dynamics of Curved Interfaces*, Pierre Pelcé (ed) (Academic Press, Inc., New York, 1988); J.D. Weeks & W. van Saarloos, Phys. Rev., **A39**, 2772 (1989); G.J. Merchant & S.H. Davis, Phys. Rev. Lett., **63**, 573 (1989); J. Bechhoefer and A. Libchaber, Phys. Rev. **B35**, 1393 (1987) and P. Oswald, J. Physique, **49**, 1083 (1988); *ibid.*, **50**, C3-127 (1989).
- [7] W. W. Mullins and R. F. Sekerka, J. Appl. Phys. **34**, 323 (1963); **35**, 444 (1964).
- [8] In these experiments, we did not intentionally add impurities to succinonitrile. What is called the crystal state here is a plastic crystal. M. A. Chopra, M. E. Glicksman and N. B. Singh, J. Cryst. Growth, **543**, 543 (1988) measure  $D=1.27 \times 10^{-5} \text{cm}^2/\text{s}$  for succinonitrile/acetone and  $D=0.88 \times 10^{-5} \text{cm}^2/\text{s}$  for succinonitrile/argon.
- [9] P. E. Cladis, J. T. Gleeson and P. L. Finn, Phys. Rev. **A44**, R6173 (1991).
- [10] Our experimental set-up is described in some detail in P. E. Cladis, J. T. Gleeson and P. L. Finn in *Defects, Patterns and Instabilities*, D. Walgraef (ed), Kluwer Academic Publishers (1990).
- [11] J. T. Gleeson et al. (unpublished). The speed,  $v$ , is constant so  $d_u$  is the product of  $v$  and the time for the cellular pattern to appear when  $v > v_{cb}$ . As  $v \rightarrow v_{cb}$ ,  $d_u \rightarrow \infty$ . And when  $v < v_{cb}$ ,  $d_u$  is undefined: the planar interface is stable. This method is useful if the interface becomes unstable everywhere at the same time which it does when  $v \approx 3v_{cb}$ .
- [12] B. Caroli, C. Caroli and B. Roulet, J. Phys. (Paris), **43**, 1767 (1982).
- [13] We use "propagate" for the groove pattern in the sense that the envelope of the groove pattern moves continuously across the interface while a



single groove keeps its place on the interface.

- [14] S. de Cheveigné, C. Guthmann and M. M. Lebrun, *J. Phys. (Paris)*, **47**, 2095 (1986).
- [15] M. J. Bennett and R. A. Brown, *Phys. Rev.* **B39**, 11705 (1989); N. Ramprasad, M. J. Bennett and R. A. Brown, *Phys. Rev.* **B38**, 583 (1988) and K. Tsiveriotis and R. A. Brown, *Phys. Rev. Lett.* **63**, 2048 (1989).
- [16] G. Dee and J. S. Langer, *Phys. Rev. Lett.*, **50**, 383 (1983); W. van Saarloos, *Phys. Rev.* **A39**, 6367 (1990).
- [17] L. Kramer, E. Ben-Jacob, H. R. Brand and M. C. Cross, *Phys. Rev. Lett.* **49**, 1891 (1982).
- [18] P. Coulet, R. E. Goldstein and G. H. Gunaratne, *Phys. Rev. Lett.*, **63**, 1954 (1989); R. E. Goldstein, G. H. Gunaratne, L. Gil and P. Coulet, *Hydrodynamic and Interfacial Patterns with Broken Space-Time Symmetry*. [preprint].
- [19] C. Misbah, *J. Phys. (Paris)* **50**, 971 (1989).
- [20] P. Oswald, J. Bechhoefer and A. Libchaber, *Phys. Rev. Lett.* **58**, 2318 (1987).
- [21] J. T. Gleeson, P. L. Finn and P. E. Cladis, *Phys. Rev. Lett.*, **66**, 236 (1991).
- [22] A. J. Simon, J. Bechhoefer and A. Libchaber, *Phys. Rev. Lett.* **61**, 2574 (1988).